Europe PMC Funders Group
Author Manuscript
Thromb Haemost. Author manuscript; available in PMC 2013 October 29.

Published in final edited form as:
Thromb Haemost. 2013 March ; 109(3): . doi:10.1160/TH12-10-0721.

Non-Invasive Imaging for Studying Anti-Angiogenic Therapy Effects

Josef Ehling[1,2], **Twan Lammers**[1,3], and **Fabian Kiessling**[1]

[1]Department of Experimental Molecular Imaging, Medical Faculty and Helmholtz Institute for Biomedical Engineering, RWTH Aachen, Aachen, Germany [2]Institute of Pathology, Medical Faculty, RWTH Aachen, Aachen, Germany [3]Department of Targeted Therapeutics, MIRA Institute for Biomedical Technology and Technical Medicine, University of Twente, Enschede, The Netherlands

Abstract

Noninvasive imaging plays an emerging role in preclinical and clinical cancer research and has high potential to improve clinical translation of new drugs. This article summarizes and discusses tools and methods to image tumor angiogenesis and monitor anti-angiogenic therapy effects. In this context, micro-computed tomography (CT) is recommended to visualize and quantify the micro-architecture of functional tumor vessels. Contrast-enhanced ultrasound (US) and magnetic resonance imaging (MRI) are favorable tools to assess functional vascular parameters, such as perfusion and relative blood volume. These functional parameters have been shown to indicate anti-angiogenic therapy response at an early stage, before changes in tumor size appear. For tumor characterization, the imaging of the molecular characteristics of tumor blood vessels, such as receptor expression, might have an even higher diagnostic potential and has been shown to be highly suitable for therapy monitoring as well. In this context, US using targeted microbubbles is currently evaluated in clinical trials as an important tool for the molecular characterization of the angiogenic endothelium. Other modalities, being preferably used for molecular imaging of vessels and their surrounding stroma, are photoacoustic imaging (PAI), near-infrared fluorescence optical imaging (OI), MRI, positron emission tomography (PET) and single photon emission computed tomography (SPECT). The latter two are particularly useful if very high sensitivity is needed, and/or if the molecular target is difficult to access. Carefully considering the pros and cons of different imaging modalities in a multimodal imaging setup enables a comprehensive longitudinal assessment of the (micro)morphology, function and molecular regulation of tumor vessels.

Keywords

angiogenesis; functional imaging; molecular imaging; vessel normalization; cancer therapy

Introduction

Angiogenesis is one of the hallmarks of cancer and anti-angiogenic therapy concepts play an important role in modern tumor treatment [1-2]. Tumors above a critical size of 2-3 mm^3 are strongly dependent on the active recruitment of new blood vessels [3-4]. Tumor angiogenesis is regulated by a plurality of proteins including pro-angiogenic factors, growth factor receptors and ECM-binding proteins like integrins [5]. Furthermore, the vascular

Corresponding author: fkiessling@ukaachen.de Department of Experimental Molecular Imaging Pauwelsstraße 30 52074 Aachen Germany Phone: +49-241-8080116 Fax: +49-241-8082006.

Europe PMC Funders Author Manuscripts
Europe PMC Funders Author Manuscripts

Europe PMC Funders Author Manuscripts

network in tumors differs significantly compared to normal tissue with respect to its high microvessel density and its chaotic organization including a high number of dysfunctional vessels [6]. With vascular imaging, tumors can be distinguished from normal tissues on the basis of morphological features, the function of blood vessels and the specific expression of angiogenesis-related markers. Thus, imaging of angiogenesis can be divided in three major areas: micro-morphological, functional and molecular imaging.

Monitoring anti-angiogenic therapy effects has become more and more important for the translation of new therapies into the clinic and for assessing therapeutic effects in individual patients. Histopathological techniques are invasive and usually do not provide information about the function of tumor vessels. Therefore, these are often supplemented by noninvasive imaging techniques, which enable the longitudinal and non-invasive evaluation of anti-tumorigenic and anti-angiogenic therapy effects [7]. In this context, the major motivation for non-invasive imaging in both, preclinical and clinical settings is to visualize, characterize and quantify tumor growth, angiogenesis and metastases at the micro-morphological, functional and molecular level [8-9]. Furthermore, the non-invasive characterization of tumor vessels leads to a better understanding of therapy effects and helps to optimize and personalize therapeutic interventions. Finally, non-invasive imaging is an important link between preclinical research and clinical application, and facilitates translational (anti-) angiogenesis research.

Current (pre-)clinically used imaging modalities include computed tomography (CT), magnetic resonance imaging (MRI), ultrasound (US), photoacoustic imaging (PAI), positron emission tomography (PET), single photon emission computed tomography (SPECT) and optical imaging (OI). In this article, an overview of current non-invasive imaging modalities will be given with respect to imaging of tumor angiogenesis (Table 1-4). Additionally, their potential for monitoring anti-angiogenic therapy effects on the micro-morphological (Figure 1), functional (Figure 2) and molecular (Figure 3) level will be discussed.

Computed Tomography

Due to its excellent spatial resolution, CT imaging enables a fast and user-independent acquisition of morphological information on tumor growth and metastatic spread. In combination with contrast-enhancement, morphological and functional imaging of tumor microvessels is feasible at very high resolution. After intravenous administration of an iodine-containing blood pool contrast agent, functional blood vessels in tumors can be visualized and quantified non-invasively using this X-ray-based technique. In such setups, contrast-enhanced CT imaging enables a high-resolved visualization and accurate quantification of angiogenic parameters like vessel size, relative blood volume (rBV), 3D distribution of vessels and vessel branching.

CT imaging of tumor growth and metastatic spread, and the non-invasive characterization of tumors based on their specific perfusion characteristics after contrast agent administration in dynamic measurements, is frequently used in the clinic [10-12]. *In vivo* μCT devices with increased spatial resolution also have enormous potential for monitoring and understanding tumor angiogenesis and anti-angiogenic therapy effects in small animal research. In this context, gantry-based and non-gantry-based μCT scanners are available. Gantry-based μCT scanners are usually preferred for fast *in vivo* imaging (e.g. with contrast agents), while non-gantry-based systems are applied to generate images of high spatial resolution (below 10 μm per voxel) taking into account long scan times and high X-ray doses. Nevertheless, few studies have been reported where vascular studies of the brain were imaged using non-gantry-based systems with acceptable scan times of 20 - 40 s [13-14]. Scan times of gantry-based μCT scanners depend on the scan protocol and contrast agent and roughly range

Europe PMC Funders Author Manuscripts

Europe PMC Funders Author Manuscripts

between 4 s and 30 min in small animal imaging studies. This results in tolerable X-ray doses between 20 and 300 mGy, and a spatial resolution ranging between 20 and 200 μm voxel side length (Figure 1A) [15].

A rapid but precise visualization of blood vessels significantly depends on the chosen contrast agent. Due to their small size, clinically used contrast agents extravasate and CT angiography imaging has to be done during the first circulations in the body. However, due to the high viscosity of CT contrast agents, this often leads to complications during i.v. injection and sometimes even to vessel rupture in small animals. Alternatively, experimental and commercial polyiodinated triglyceride emulsions with long blood half-life times are available [16-18]. However, when using blood pool CT contrast agents care should be taken to assure that the iodine concentration in the injection solution is sufficiently high (based on our own experience at least 130 mg iodine per ml are required for the visualization of microvessels). In such cases, the intravenous administration of the contrast agent can be performed prior to the μCT scan, if the scan is performed immediately afterwards [19]. Alternatively, for dynamic analyses, a catheterization of the animals enables a constant application (infusion) of the contrast agent during the scan, allowing a more complex pharmacokinetic analysis and the extraction of additional functional parameters. Dynamic contrast-enhanced μCT (DCE- μCT) imaging was for instance performed by Eisa and colleagues, who investigated the anti-angiogenic effect of the mTOR inhibitor Afinitor (everolimus) in orthotopic MCF-7 mammary cancer xenografts [20]. After mice had undergone DCE- μCT, functional parameters like the rBV, vascular permeability (*K*) and area under the time-enhancement curve (AUC) were calculated for the total, peripheral and central tumor volumes of interest (Figure 2A). They could demonstrate that the mean AUC was significantly lower in Afinitor-treated tumors than in control tumors. However, significant differences for rBV and *K* could only be observed for peripheral tumor regions. In another experimental setting, Tai et al. investigated the effects of the multi-tyrosine kinase inhibitor vandetanib in subcutaneous LoVo human colon carcinoma-bearing nude rats using DCE- μCT. It was shown that 24 h after the therapy started, vandetanib significantly reduced tumor blood flow (BF) and rBV, but not mean transit time (MTT) and vascular permeability; vehicle treatment had no significant effect on the determined parameters [21]. An overview of vascular parameters that can be assessed using contrast-enhanced μCT is given in table 3. However, by using DCE- μCT, it should be taken into consideration that this technique still suffers from beam hardening artifacts originating e.g. from bones or highly contrasted large vessels.

For analyzing microvessels in bone metastases, and for distinguishing between radiopaque bone structures and contrast-enhanced microvessels, dual-energy CT approaches can be applied, both, preclinically and clinically [22-23]. Dual-energy CT is based on two X-ray beams with different energy compositions. Due to X-ray energy-dependent absorption characteristics of bone structures and contrast-enhanced blood vessels, blood vessels can be specifically detected and quantified even inside radiopaque bone structures. The dual energy μCT technique was for example applied by Gremse et al., who used it to assess vascular inflammation and stenosis in mice [24].

High-resolution *ex vivo* μCT imaging techniques can be used for generating and analyzing 3D images of the micro-architecture of the tumor vasculature with a spatial resolution of less than 5 μm voxel side length. For this approach, Savai and colleagues perfused mice with orthotopic lung carcinoma tumors with Microfil® (i.e. a lead-containing silicone rubber suspension, which polymerizes intravascularly). After tumor harvesting and scanning in a high-resolution μCT system, a significant reduction of small blood vessels was observed in bevacizumab-treated vs. untreated tumors [25]. Such casting methods provide important information on the 3D micro-morphology of the tumor vasculature, enabling e.g. the

Europe PMC Funders Author Manuscripts

Europe PMC Funders Author Manuscripts

assessment of blood vessel size, blood vessel distribution and blood vessel branching (3D morphology of tumor microvessels is exemplified in an A549 human lung adenocarcinoma xenograft in Figure 1B).

Alternatively, intravital microscopy approaches such as multiphoton microscopy (MPM) and optical frequency domain imaging (OFDI) using tumors grown in dorsal skin fold chambers can be used for such purposes, i.e. for studying the 3D micro-morphological aspects of tumor angiogenesis. The dorsal skin fold chamber technique was initially described in rats by Papenfuss and colleagues [26] and was used for long-term imaging of tumor blood vessels for instance by Leunig and Lichtenfeld [27-28]. Using this technique, a detailed comparison between MPM and OFDI for investigating the micro-architecture of tumor blood vessels *in vivo* was performed by Vakoc and colleagues [29]. In particular using OFDI, they showed that the VEGFR-2 blocking monoclonal antibody DC101 longitudinally leads to a significant reduction of mean intratumoral vessel length and diameter in murine mammary adenocarcinoma tumor xenografts. Surprisingly, angiogenesis-related parameters like tortuosity or fractal dimension did not alter upon treatment [29]. The cranial window model is another technique for long-term intravital imaging of blood vessels of cerebral tumors exploiting a high optical transparency. This model was, for instance, used by Hansen-Algenstaedt and colleagues for the non-invasive visualization of tumor blood vessels in tumor xenografts of the brain [30].

Magnetic Resonance Imaging

Advantages of MRI are its high spatial resolution, excellent soft tissue contrast and a broad arsenal of methods that can be applied to functionally characterize tissues. The latter include both, non contrast-enhanced techniques, such as spectroscopy (MRS; to investigate cell metabolism), diffusion weighted imaging (DWI; measuring cellularity), time of flight (TOF) angiography, arterial spin labeling (ASL; to visualize vessels and monitor perfusion), blood oxygenation level dependent imaging (BOLD; to assess vessel oxygenation, vessel responsiveness and maturity), as well as contrast enhanced methods like dynamic contrast enhanced MR imaging (DCE-MRI, to assess rBV, perfusion and permeability) and vessel size imaging (VSI; to quantify the mean vessel diameter within tissues) [31].

DWI and MRS are methods to assess tissue cellularity and metabolism and there are a number of review articles about their use for cancer characterization [32-33]. ASL is based on radiofrequency pulses which excite the nuclear spin of inflowing arterial protons, resulting in magnetic labeling of the inflowing blood. Using this endogenous contrast, ASL can be used to assess blood flow and tissue perfusion. Similarly, TOF angiography visualizes vessels by the signal change that occurs when magnetized protons in the blood leave the image voxel during the measurement [34]. Although the non-contrast-enhanced visualization of tumor vessels by TOF and ASL improves when using MRI devices operating at higher field strength, vessels with very slow blood velocities cannot be reliably depicted (cf. Doppler ultrasound). Since especially these vessels respond to anti-angiogenic therapies, contrast-enhanced T1-weighted angiography and DCE-MRI are generally preferred for therapy monitoring.

Using MR angiography in combination with gadolinium-based blood pool contrast agents, vessels as small as 30 - 100 □m in diameter can be visualized [14, 31, 35]. DCE-MRI in combination with quantitative pharmacokinetic analyses provides information on vascular parameters like blood flow, rBV, regional distribution volume of the contrast agent (rDV), MTT, tissue perfusion and changes in vessel permeability (cf. table 3). In this context, it was demonstrated that DC101-induced changes in the rBV of human skin squamous cell carcinomas in mice could be assessed by Gd-DTPA-enhanced dynamic T1-weighted MRI

Europe PMC Funders Author Manuscripts

Europe PMC Funders Author Manuscripts

before changes in tumor size became apparent (Figure 2C) [36]. In addition to subcutaneous tumors, DCE-MRI has also been shown to work reliably for monitoring orthotopic tumors and even metastases [37-38]. DCE-MRI has furthermore been successfully applied in several clinical trials focusing on anti-angiogenic therapy, e.g. in investigating the therapeutical effects of PTK/ZK (a VEGFR tyrosine kinase inhibitor) in patients with colorectal cancer and liver metastases, of axitinib (AG-013736; a multi-target tyrosine kinase inhibitor) in patients with advanced solid tumors, and of bevacizumab in patients with breast cancer [39-41].

An MRI technique capable of obtaining anatomical information of blood vessels on the micro-morphological scale is vessel size imaging (VSI). VSI is based on the measurement of T2 and T2* relaxation times before and after the intravenous injection of a superparamagnetic contrast agent. While the T2 relaxation time is dependent on water diffusion, and therefore on the size and number of vessels per voxel, changes in the T2* relaxation time are mostly dependent on the amount of contrast agent per voxel. With these two pieces of information, it is possible to calculate the mean vessel diameter of tissues [42]. Reports on the changes of mean vessel diameters in tumors during anti-angiogenic therapy have provided contradictory results. On the one hand, investigating the anti-angiogenic effects of sunitinib in A431 xenografts and of bevacizumab in HaCaT-ras-A-5RT3 xenografts, Zwick and colleagues analyzed treatment-induced changes in tumor vascularity by DCE-MRI and VSI [43]. In both tumor models, the mean vessel size increased as a result of therapy, which can be explained by the fact that the vessels responding to treatment are mostly small and immature, and that larger and more mature vessels persist after therapy. On the other hand, when using the vascular disrupting agent ZD6126 to treat prostate cancer xenografts, decreases in vessel size indices were observed [44]. Reasons might be differences in the vascular architecture in the different tumor models used (e.g. larger immature vessels), or differences in the mechanism of action of the anti-vascular agents used.

Another approach for longitudinally analyzing anti-angiogenic therapy effects in tumors dependent on vessel maturation is BOLD MRI. The BOLD contrast derives from the different relaxation characteristics of oxygenated and de-oxygenated hemoglobin in the blood. The inhalation of oxygen can be used to induce a signal change in the blood and thus to characterize tissue vascularization. Also the response of vessels to hypercapnia vs. hyperoxia can be studied. By this, information about vascular maturity is obtained since only mature vessels associated with periendothelially localized contractile mural cells functionally respond to elevated levels of CO_2 (hypercapnia). As an example, inhaling air with a CO_2 content of 5% leads to a selective contraction of mature vessels, which results in specific MR signal changes [45-46]. In a novel approach, Cai and co-workers investigated the BOLD effect under different levels of oxygen inhalation for the development of MR BOLD angiography (Figure 1 G-H) [47].

For molecular imaging, numerous molecular MR probes have been developed to monitor tumor angiogenesis. Among the most frequently used ones are antibody- or peptide-coated ultrasmall superparamagnetic iron oxide nanoparticles (USPIOs) [48-49] and Gd-loaded paramagnetic liposomes [50-51]. The design, structure and application of different types of MR contrast agents are reviewed in [52]. In addition, there are few reports on low-molecular-weight probes binding to integrins [53], thrombin, fibrin or elastin [54]. Although it has been shown that using RGD-coated USPIO, squamous cell carcinomas with high vs. low levels of integrin expression on tumor blood vessels can be distinguished [55], and that anti-angiogenic therapy effects can be monitored with paramagnetic liposomes [51], there still is a debate on the reliability of the method and its usefulness for biological and medical research.

Europe PMC Funders Author Manuscripts

Europe PMC Funders Author Manuscripts

Ultrasound Imaging

Ultrasound is one of the most frequently used tomographic clinical imaging modalities. In preclinical settings, high-frequency US enables a real-time acquisition of functional and molecular information with high temporal and spatial resolution.

Power Doppler US is used as a method for studying anti-angiogenic therapy effects based on echo frequencies coming from moving elements, e.g. circulating blood cells. For this technique, no contrast agent has to be injected (Figure 1E). It allows the quantification of blood flow and the visualization of tumor vascularization. However, it should be noted that the sensitivity of Power Doppler US is not sufficient to depict small vessels (<100 □m) with low flow velocities [56]. In particular, this has to be seen critical if anti-angiogenic therapy effects should be assessed and quantified in tumors, which contain mainly small and immature blood vessels with slow flow velocities. Nevertheless, several groups have been able to demonstrate that contrast-enhanced Power Doppler US is capable of quantifying anti-angiogenic therapy effects in preclinical *in vivo* tumor models [57-59].

With the help of gas-filled microbubbles (MB), the assessment of the architecture of tumor blood vessels as well as of functional or molecular parameters can be improved (Figure 1F). Gas-filled MB increase the difference in the acoustic impedance between contrast-enhanced and non-enhanced tissues, and can be detected with high sensitivity and specificity [56]. Unspecific gas-filled MB are used as a contrast agent for the visualization (Figure 1 C-D) and quantification of blood velocity, perfusion and the relative blood volume (rBV) (Figure 2B) in tumors [60-61]. Specific antibody- or peptide-modified MB are used for molecular US imaging of angiogenesis-related markers (Figure 3A-C).

After the intravenous injection of MB, which remain strictly intravascular because of their large size, the following parameters are generally calculated from the signal intensity vs. time curve: the maximum peak enhancement, the up-slope, the delay time and the area under curve. It has been shown that the maximum peak in color pixel density and the accumulated maximum intensity over time correlate well with the rBV in tumors, and that the up-slope of the intensity curve correlates with perfusion [56]. Based on these parameters, several studies have been performed employing contrast-enhanced functional US for the quantification of anti-angiogenic therapy effects, showing a significant correlation in the assessment of therapy response with post-mortem histology. The tumor rBV was determined from the change in signal intensity after MB injection, indicating in the vast majority of cases that anti-angiogenic therapies lead to significant reduction of rBV in comparison to non-treated animals, and that these effects correlate with the microvessel density (MVD) determined by histology [56, 62-63]. Palmowski and colleagues used a combination of 3D non-contrast-enhanced and contrast-enhanced Power Doppler US for longitudinal monitoring anti-angiogenic effects of sunitinib in A431 epidermoid carcinoma-bearing mice. Because contrast-sensitive US recognizes all vessels, whereas flow-sensitive non-contrast-enhanced Doppler US predominantly captures mature vessels, a selective response of different vessel fractions and thus vascular maturation during anti-angiogenic therapy could be assessed (Figure 2B) [64].

Another method to quantify rBV and perfusion is via destruction-replenishment analysis. This is based on the destruction of MB at a stable blood concentration phase in the imaged area by high-energy US pulses and on the subsequent measurement of the re-entry of circulating MB into the vascularized region of interest. This enables the quantification of blood velocity and perfusion. Krix and co-workers adapted this method to be applicable after bolus injection of MB and showed in squamous cell carcinoma xenografts that effects of the anti-VEGFR-2 antibody DC101 can be mirrored faithfully [65].

Europe PMC Funders Author Manuscripts

Europe PMC Funders Author Manuscripts

Molecular US imaging is frequently applied to non-invasively study tumor angiogenesis and anti-angiogenic therapy effects. During tumor growth, receptor structures such as VEGFR-2 or $\alpha_v\beta_3$ integrins are highly overexpressed on endothelial cells within tumor blood vessels. For molecular US imaging, MB can be functionalized with targeting moieties which enable specific binding to these endothelial cell markers upon intravenous MB administration (Figure 3A). Different procedures for labeling MB with specific antibodies or peptides have been described, based either on the direct incorporation or chemical coupling, or indirectly via strept(avidin)-biotin interactions [56, 66-67]. The specific accumulation of targeted MB at pathological sites can be assessed by a signal subtraction method (pre minus post a destructive pulse, Figure 3B) or by Sensitive Particle Acoustic Quantification (SPAQ, Figure 3C) [56]. Molecular US imaging sensitively indicated changes in VEGFR-2 or $\alpha_v\beta_3$ integrin expression during therapeutic inhibition of matrix metalloproteinases [68] and early vascular inflammation after heavy ion therapy using MB targeted to ICAM-1 and $\alpha_v\beta_3$ integrin [69-70]. However, since such molecular information generally does not allow differentiation between changes in marker expression on the endothelial surface and changes in blood vessel density in tumors, functional and molecular US should be combined, and a normalization of the molecular data on the basis of the functional data (rBV) should be performed [71].

Optical and Photoacoustic Imaging

Optical imaging is based on the detection of light, which is emitted from injectable probes or heterologous proteins inside the body after illumination with excitation light. Emission wavelengths of the near-infrared fluorochromes ranging between 650-950 nm are generally preferred, resulting in minimized tissue absorption and low levels of autofluorescence. Several planar and tomographic near-infrared fluorescence OI modalities have been developed in the last decade, primarily for the *in vivo* monitoring of molecular targets. In this context, planar optical reflectance imaging (ORI) systems allow semi-quantitative analyses, while tomographic methods such as fluorescence molecular tomography (FMT) are more quantitative and less penetration depth-dependent, resulting in a spatial resolution of 1 mm voxel side length [72]. However, due to the lack of morphological information, it is a great advantage to choose a hybrid optical imaging approach as presented in [73-74], in order to have better anatomical assignment of the fluorescent signals, and to improve optical image reconstruction by considering information from the mouse anatomy.

Several optical blood pool agents [75-76] as well as optical probes targeting VEGFR-2 or $\alpha_v\beta_3$ integrin in tumors [77-79] have been designed and evaluated, and have demonstrated the potential of planar and tomographic OI for monitoring the efficacy of anticancer therapy. For instance, Lederle et al. used an annexin-based fluorescent probe to monitor apoptosis in A431 epidermoid carcinoma xenografts treated with sunitinib using FMT (Figure 3D). Additionally, tumor vascularization was investigated by FMT using an optical blood pool marker and by contrast-enhanced US. Vascularization significantly decreased in treated tumors, however no enhanced annexin accumulation was observed although the gold standard TUNEL staining indicated increased apoptosis. It was shown that the rapid breakdown of vascularization during anti-angiogenic therapy impaired the delivery of annexin and thus resulted in seemingly lower apoptosis rates [76]. This clearly shows that molecular imaging of extravascular targets can fail if vascular physiology dramatically changes and illustrates the need to acquire both, functional and molecular information in order to avoid data misinterpretation.

Bioluminescence imaging (BLI) enables the non-invasive and longitudinal assessment of tumor growth, metastasis, angiogenesis and gene expression *in vivo* using a reporter gene approach. In this context, the bioluminescent reporter system is mainly luciferase reacting

Europe PMC Funders Author Manuscripts

Europe PMC Funders Author Manuscripts

with a substrate (e.g. luciferin) and resulting in emitted light with an emission spectrum between 480 nm and 611 nm. An overview of bioluminescence instruments, gene reporter systems and fluorescent probes is given by Snoeks et al. [80]. For studying effects of VEGFR-2 on tumor angiogenesis and for monitoring VEGFR-2 gene expression *in vivo*, Zhang and colleagues established a VEGFR-2-luciferase transgenic mouse model (FVB/NTg(VEGFR2-luc)-Xen) [81]. Red and green fluorescent tumor cells were inoculated in a VEGFR2-luc knock-in mouse, enabling the simultaneous imaging and quantification of tumor growth, as well as the non-invasive assessment of angiogenesis [80]. For similar purposes, transgenic mouse models expressing GFP [82] or luciferase under control of the VEGF promoter [83] are available, as well as Tie2-GFP and eNOS-GFP reporter mice [80].

Due to the fact that during tumor growth, hypoxia and the subsequent stabilization of hypoxia inducible factor-1 (HIF-1) play key roles in the induction of angiogenesis, several luciferase or GFP reporter constructs were established which are driven by the hypoxia responsive element (HRE), i.e. the HIF-1 target binding site. These HRE-reporter constructs have been demonstrated to be valuable tools to non-invasively evaluate tumor hypoxia and the efficacy of hypoxia-directed therapies [80].

Photoacoustic imaging (PAI) is a relatively young imaging technique, which is based on the thermoelastic expansion of molecules after light absorption and thus the conversion of optical to ultrasonic energy. PAI can provide morphological, functional, and molecular information and even fluorescent reporter genes can be used [84]. Due to its strong optical absorption, hemoglobin can be used as an intrinsic contrast agent to visualize vessels in combination with quantitative functional information on absolute blood oxygen saturation and blood flow [85]. De la Zerda and co-workers investigated first the potential of PAI in preclinical tumor models for the visualization and quantification of tumor angiogenesis using novel photoacoustic contrast agents that are based on the binding of small optical dyes and RGD peptides to single-walled carbon nanotubes (SWNT-dye) [86]. For investigation of the potential of PAI for the *in vivo* visualization and quantification of tumor angiogenesis and tumor growth at the microscopic level, Cai and colleagues inoculated lacZ-marked 9 L gliosarcoma tumor cells into mice. Tumors were non-invasively and simultaneously imaged by dual-wavelength acoustic-resolution photoacoustic microscopy: lacZ-expressing tumor cells by optical imaging at a 635 nm wavelength and the tumor surrounding microvasculature by photoacoustic imaging at a 584 nm wavelength [87]. These data suggest that PAI may establish as a complementary tool to conventional optical fluorescence imaging of reporter genes for the *in vivo* assessment of therapy effects on total tumor volume and tumor microvasculature. PAI is a translational imaging modality and first clinical studies have demonstrated its potential application for imaging melanoma tumors, gastrointestinal tract endoscopy, intravascular catheter imaging, neonatal brain imaging, breast cancer detection, prostate cancer detection, sentinel lymph node imaging, blood perfusion and oxygenation imaging [84].

Positron Emission Tomography and Single Photon Emission Computed Tomography

For the identification and quantification of molecular processes and targets involved in the development and progression of cancer and tumor angiogenesis at the picomolar to nanomolar level, positron emission tomography (PET) and single photon emission computed tomography (SPECT) are the modalities of choice. Both play a major role in the preclinical development of novel targeted drugs and in clinical cancer diagnosis and therapy monitoring. While PET is based on the co-incidence of two γphotons with 511 keV, SPECT measures single gamma photons with isotope-specific energies (e.g. ^{99m}Tc, ^{111}In, ^{123}I and ^{201}TI). This enables measuring different tracers simultaneously and also tracers with a

Europe PMC Funders Author Manuscripts

Europe PMC Funders Author Manuscripts

broader range of half-lives are available. However, sensitivity of SPECT is lower than for PET and it is less quantitative.

For molecular imaging of tumor angiogenesis using PET, a number of radioactive tracers targeting angiogenesis-related markers such as growth factors, tyrosine kinase receptors and integrins, have been developed (for a detailed overview of radiolabeled anti-VEGF/VEGFR and anti- $\alpha_v\beta_3$ tracers, see Cai et al. [88]). As an example, $VEGF_{121}$ was radiolabeled with ^{64}Cu, and it was demonstrated that ^{64}CU-DOTA-$VEGF_{121}$ had a rapid and specific uptake in highly vascularized small U87MG glioma xenografts, with high levels of VEGFR-2, and a significantly lower uptake in large U87MG tumors, which expressed low levels of VEGFR-2 [89]. Also SPECT imaging of VEGF receptors was described to characterize tumor angiogenesis and to assess anti-angiogenic therapies in several preclinical approaches [88].

In several studies, PET radiotracers with ^{18}F-, ^{68}Ga-, and ^{64}Cu-labeled RGD were utilized for $\alpha_v\beta_3$ integrin imaging, to quantify angiogenesis at the molecular level [90-91]. Similarly, ^{99m}Tc-labeled RGD probes were used to assess $\alpha_v\beta_3$ expression in experimental gliomas [92]. Yang et al. treated orthotopic MDA-MB-435 tumor-bearing mice with the VEGFR-2 tyrosine kinase inhibitor ZD4190 and could demonstrate that the proliferation-specific ^{18}F-FLT and integrin-specific ^{18}F-FPPRGD2 uptake in tumors treated with ZD4190 were significantly lower than in control animals, and correlated with immunohistochemical findings from CD31, CD61 and Ki-67 stainings [93]. In another study, Jin and co-workers demonstrated that integrin imaging by ^{64}Cu-cyclam-RAFT-c(-RGDfK-)4 PET indicates response of human hepatocellular carcinoma xenografts to a novel multi-targeted tyrosine kinase inhibitor, and that the change in tracer uptake correlates well with histological microvessel density [94].

In the clinical context, anti-angiogenic therapy effects are mostly assessed using clinically established radiotracers, reporting on tumor cell metabolism and proliferation. For example, ^{18}F-FDG PET (indicating glucose uptake and hexokinase activity) was used for therapy monitoring of GIST (gastrointestinal stromal tumors) in patients treated with imatinib or sunitinib [95]. In a recent clinical study focusing on glioma treatment with bevacizumab, Schwarzenberg and co-workers demonstrated that ^{18}F-FLT PET is a sensitive indicator of therapy response and that a change in tracer uptake is a decent indicator of progression-free survival (Figure 3E) [96]. In a molecular approach, Metz and co-workers examined patients with primary or metastasized lung cancer with DCE-MRI and with PET using ^{18}F-galacto-RGD and ^{18}F-FDG PET. They could demonstrate that an early therapy response can be assessed by PET imaging using ^{18}F-galacto-RGD but not ^{18}F-FDG tracers, and that these data correlate with findings from DCE-MRI [97]. In breast cancer patients using SPECT, Bach-Gansmo and co-workers investigated the potential of the integrin-specific ^{99m}Tc-NC100692 tracer and could demonstrate that 19 of 22 malignant lesions were detected using ^{99m}Tc-NC100692 scintigraphy [98]. In a theranostic approach, the accumulation of ^{11}C-docetaxel after administration of bevacizumab was studied, in order to investigate whether vascular normalization induced by VEGF-inhibition leads to a better accumulation of the radiolabelled drug. Unfortunately, the opposite was observed, clearly demonstrating the need for individual therapy scheduling and optimized dosing of anti-angiogenic drugs in combination therapy schedules [99].

Conclusions

Over the last years, many promising non-invasive imaging techniques have been developed which enable a reliable characterization of blood vessels within tumors. Many of these techniques could be translated to the clinic and now form an important link between

Europe PMC Funders Author Manuscripts

Europe PMC Funders Author Manuscripts

preclinical and clinical cancer research. In this context, it has clearly been shown that noninvasively determined functional and/or molecular vascular parameters are often earlier and more reliable indicators of therapy response than tumor size measurements. Nevertheless, the optimal implementation of non-invasive angiogenesis imaging into preclinical research and clinical diagnosis (for therapy monitoring) can only occur if the obtained parameters are clearly understood in relation to the underlying tumor biology. Functional and molecular parameters are often required together to understand vascular remodeling. This does not always require a multimodal but often a multi-parametric approach. In this context, the choice of tools should be based on the aim to combine the best working modalities and methods providing the most reliable quantitative measures, thereby generating minimal costs and requiring as less time as possible. In particular for facilitating clinical translation and for individualizing (chemo-) therapeutic interventions, it is of significant importance to adapt the therapeutic protocol (e.g. choice of drug, dosing regimen, treatment change, etc) on the basis of the results obtained using non-invasive imaging. Such theranostic concepts, i.e. direct and tight combinations of disease diagnosis and therapy, are considered to be highly important for realizing the potential of personalized medicine.

Acknowledgments

The authors gratefully acknowledge the German Federal State of North Rhine Westphalia (NRW; HighTech.NRW / EU-Ziel 2-Programm (EFRE); ForSaTum), the European Union (European Regional Development Fund - Investing In Your Future; and COST-Action TD1004), the European Research Council (ERC-StG-309495-NeoNaNo), and the German Research Foundation (DFG; EH 412/1-1 and LA 2937/1-1) for financial support.

Abbreviations

A	amplitude
ASL	arterial spin labeling
a.u.	arbitrary units
AUC	area under curve
BF	blood flow
BLI	bioluminescence imaging
BOLD	blood oxygenation level dependent
^{11}C	^{11}carbon
CD31	cluster of differentiation 31 (platelet endothelial cell adhesion molecule 1, PECAM-1)
CD61	cluster of differentiation 61 (integrin ß3)
cf.	*confer* (compare)
CO_2	carbon dioxide
^{64}Cu	^{64}copper
3D	three-dimensional
DCE- CT	dynamic contrast-enhanced micro-computed tomography
DCE-MRI	dynamic contrast-enhanced magnetic resonance imaging
DOTA	1,4,7,10-tetraazacyclododecane-1,4,7,10-tetraacetic acid
DWI	diffusion weighted imaging

Europe PMC Funders Author Manuscripts

Europe PMC Funders Author Manuscripts

e.g.	*exempli gratia* (for example)
eNOS	endothelial nitric oxide synthasis
et al.	*et alii* (and others)
^{18}F	^{18}fluorine
^{18}F-FDG	^{18}F-fluoro-desoxy-glucose
^{18}F-FLT	3-deoxy-3-^{18}F-fluorothymidine
^{18}F-FPPRGD2	^{18}fluorine 2-fluoropropionyl labeled PEGylated dimeric RGD peptide
FMT	fluorescence molecular tomography
^{68}Ga	^{68}gallium
Gd	gadolinium
Gd-DTPA	gadolinium diethylenetriaminepentacetate
GFP	green fluorescent protein
GIST	gastrointestinal stromal tumor
HIF-1	hypoxia-inducible factor 1
HRE	hypoxia response element
ICAM-1	intercellular adhesion molecule 1
i.e.	*id est* (that is)
^{123}I	^{123}iodine
^{111}In	^{111}indium
K	vascular permeability
K_{ep}	exchange rate constant
keV	kilo electron volt
lacZ	β-galactosidase encoding gene
MB	microbubbles
(μ)CT	(micro-) computed tomography
mGy	milligray
MRI	magnetic resonance imaging
mTOR	mammalian target of rapamycin
MTT	mean transit time
MPM	multiphoton microscopy
MRS	magnetic resonance spectroscopy
MRSI	magnetic resonance signal intensity
MVD	microvessel density
OFDI	optical frequency domain imaging
OI	optical imaging
ORI	optical reflectance imaging

Europe PMC Funders Author Manuscripts

Europe PMC Funders Author Manuscripts

PAI	photoacoustic imaging
PDT	photodynamic therapy
PET	positron emission tomography
PS	permeability surface area product
rBV	relative blood volume
rDV	regional distribution volume
RGD	one-letter amino acid code for Arginine-Glycine-Aspartic
SPAQ	sensitive particle acoustic quantification
SPECT	single photon emission computed tomography
SUV	standardized uptake value
SWNT	single-walled nanotubes
^{99m}Tc	^{99m} technetium
Tie2	tyrosine kinase with immunoglobulin-like and EGF-like domains 2
^{201}TI	^{201}thallium
TOF	time of flight
TUNEL	terminal deoxynucleotidyl transferase dUTP nick end labeling
US	ultrasound
USPIO	ultrasmall superparamagnetic iron oxide nanoparticle
VEGF	vascular endothelial growth factor
VEGFR-2	vascular endothelial growth factor receptor 2
VEGFR2-luc	VEGFR-2-luciferase
VOI	volume of interest
vs.	v*ersus*
VSI	vessel size imaging

References

1. Folkman J. Angiogenesis in cancer, vascular, rheumatoid and other disease. Nat Med. 1995; 1:27–31. [PubMed: 7584949]
2. Carmeliet P, Jain RK. Molecular mechanisms and clinical applications of angiogenesis. Nature. 2011; 473:298–307. [PubMed: 21593862]
3. Hanahan D, Weinberg RA. Hallmarks of cancer: the next generation. Cell. 2011; 144:646–74. [PubMed: 21376230]
4. Bergers G, Benjamin LE. Tumorigenesis and the angiogenic switch. Nat Rev Cancer. 2003; 3:401–10. [PubMed: 12778130]
5. Ferrara N. VEGF and the quest for tumour angiogenesis factors. Nat Rev Cancer. 2002; 2:795–803. [PubMed: 12360282]
6. Baluk P, Hashizume H, McDonald DM. Cellular abnormalities of blood vessels as targets in cancer. Curr Opin Genet Dev. 2005; 15:102–11. [PubMed: 15661540]
7. McDonald DM, Choyke PL. Imaging of angiogenesis: from microscope to clinic. Nat Med. 2003; 9:713–25. [PubMed: 12778170]

Europe PMC Funders Author Manuscripts

8. Miller JC, Pien HH, Sahani D, et al. Imaging angiogenesis: applications and potential for drug development. J Natl Cancer Inst. 2005; 97:172–87. [PubMed: 15687360]
9. Lederle W, Palmowski M, Kiessling F. Imaging in the age of molecular medicine: monitoring of anti-angiogenic treatments. Curr Pharm Biotechnol. 2012; 13:595–608. [PubMed: 22214504]
10. Lee TY, Purdie TG, Stewart E. CT imaging of angiogenesis. Q J Nucl Med. 2003; 47:171–87. [PubMed: 12897709]
11. d'Assignies G, Couvelard A, Bahrami S, et al. Pancreatic endocrine tumors: tumor blood flow assessed with perfusion CT reflects angiogenesis and correlates with prognostic factors. Radiology. 2009; 250:407–16. [PubMed: 19095784]
12. Ohno Y, Koyama H, Matsumoto K, et al. Differentiation of malignant and benign pulmonary nodules with quantitative first-pass 320-detector row perfusion CT versus FDG PET/CT. Radiology. 2011; 258:599–609. [PubMed: 21273522]
13. Schambach SJ, Bag S, Steil, et al. Ultrafast high-resolution in vivo volume-CTA of mice cerebral vessels. Stroke. 2009; 40:1444–50. [PubMed: 19213951]
14. Figueiredo G, Brockmann C, Boll H, et al. Comparison of digital subtraction angiography, microcomputed tomography angiography and magnetic resonance angiography in the assessment of the cerebrovascular system in live mice. Clin Neuroradiol. 2012; 22:21–8. [PubMed: 22109696]
15. Bartling SH, Stiller W, Semmler W, et al. Small animal computed tomography imaging. Curr Med Imaging Rev. 2007; 3:45–9.
16. Vera DR, Mattrey RF. A molecular CT blood pool contrast agent. Acad Radiol. 2002; 9:784–92. [PubMed: 12139092]
17. Kao CY, Hoffman EA, Beck KC, et al. Long-residence-time nano-scale liposomal iohexol for X-ray-based blood pool imaging. Acad Radiol. 2003; 10:475–83. [PubMed: 12755534]
18. De Vries A, Custers E, Lub J, et al. Block-copolymer-stabilized iodinated emulsions for use as CT contrast agents. Biomaterials. 2010; 31:6537–44. [PubMed: 20541800]
19. Kiessling F, Greschus S, Lichy M, et al. Volumetric computed tomography (VCT): a new technology for noninvasive, high-resolution monitoring of tumor angiogenesis. Nat Med. 2004; 10:1133–8. [PubMed: 15361864]
20. Eisa F, Brauweiler R, Hupfer M, et al. Dynamic contrast-enhanced micro-CT on mice with mammary carcinoma for the assessment of antiangiogenic therapy response. Eur Radiol. 2012; 22:900–7. [PubMed: 22071777]
21. Tai JH, Tessier J, Ryan AJ, et al. Assessment of acute antivascular effects of vandetanib with high-resolution dynamic contrast-enhanced computed tomographic imaging in a human colon tumor xenograft model in the nude rat. Neoplasia. 2010; 12:697–707. [PubMed: 20824046]
22. Bäuerle T, Bartling S, Berger M, et al. Imaging anti-angiogenic treatment response with DCE-VCT, DCE-MRI and DWI in an animal model of breast cancer bone metastasis. Eur J Radiol. 2010; 73:280–7. [PubMed: 19070445]
23. Granton PV, Pollmann SI, Ford NL, et al. Implementation of dual- and triple-energy cone-beam micro-CT for postreconstruction material decomposition. Med Phys. 2008; 35:5030–42. [PubMed: 19070237]
24. Gremse F, Grouls C, Palmowski M, et al. Virtual elastic sphere processing enables reproducible quantification of vessel stenosis at CT and MR angiography. Radiology. 2011; 260:709–17. [PubMed: 21788527]
25. Savai R, Langheinrich AC, Schermuly RT, et al. Evaluation of angiogenesis using micro-computed tomography in a xenograft mouse model of lung cancer. Neoplasia. 2009; 11:46–56.
26. Papenfuss HD, Gross JF, Intaglietta M, et al. A transparent access chamber for the rat dorsal skin fold. Microvasc Res. 1979; 18:311–8. [PubMed: 537508]
27. Leunig M, Yuan F, Menger MD, et al. Angiogenesis, microvascular architecture, microhemodynamics, and interstitial fluid pressure during early growth of human adenocarcinoma LS174T in SCID mice. Cancer Res. 1992; 52:6553–60. [PubMed: 1384965]
28. Lichtenbeld HC, Barendsz-Janson AF, van Essen H, et al. Angiogenic potential of malignant and non-malignant human breast tissues in an in vivo angiogenesis model. Int J Cancer. 1998; 77:455–9. [PubMed: 9663610]

Europe PMC Funders Author Manuscripts

Europe PMC Funders Author Manuscripts

29. Vakoc BJ, Lanning RM, Tyrrell JA, et al. Three-dimensional microscopy of the tumor microenvironment in vivo using optical frequency domain imaging. Nat Med. 2009; 15:1219–23. [PubMed: 19749772]
30. Hansen-Algenstaedt N, Joscheck C, Schaefer C, et al. Long-term observation reveals time-course-dependent characteristics of tumour vascularisation. Eur J Cancer. 2005; 41:1073–85. [PubMed: 15862758]
31. Kiessling F, Jugold M, Woenne EC, et al. Non-invasive assessment of vessel morphology and function in tumors by magnetic resonance imaging. Eur Radiol. 2007; 17:2136–48. [PubMed: 17308924]
32. Glunde K, Jiang L, Moestue SA, et al. MRS and MRSI guidance in molecular medicine: targeting and monitoring of choline and glucose metabolism in cancer. NMR Biomed. 2011; 24:673–90. [PubMed: 21793073]
33. Bonekamp S, Corona-Villalobos CP, Kamel IR. Oncologic applications of diffusion-weighted MRI in the body. J Magn Reson Imaging. 2012; 35:257–79. [PubMed: 22271274]
34. Wheaton AJ, Miyazaki M. Non-contrast enhanced MR angiography: physical principles. J Magn Reson Imaging. 2012; 36:286–304. [PubMed: 22807222]
35. Doblas S, He T, Saunders D, et al. Glioma morphology and tumor-induced vascular alterations revealed in seven rodent glioma models by in vivo magnetic resonance imaging and angiography. J Magn Reson Imaging. 2010; 32:267–75. [PubMed: 20677250]
36. Kiessling F, Farhan N, Lichy MP, et al. Dynamic contrast-enhanced magnetic resonance imaging rapidly indicates vessel regression in human squamous cell carcinomas grown in nude mice caused by VEGF receptor 2 blockade with DC101. Neoplasia. 2004; 6:213–23. [PubMed: 15153333]
37. Luo Y, Jiang F, Cole TB, et al. A novel multi-targeted tyrosine kinase inhibitor, linifanib (ABT-869), produces functional and structural changes in tumor vasculature in an orthotopic rat glioma model. Cancer Chemother Pharmacol. 2012; 69:911–21. [PubMed: 22080168]
38. Dafni H, Kim SJ, Bankson JA, et al. Macromolecular dynamic contrast-enhanced (DCE)-MRI detects reduced vascular permeability in a prostate cancer bone metastasis model following anti-platelet-derived growth factor receptor (PDGFR) therapy, indicating a drop in vascular endothelial growth factor receptor (VEGFR) activation. Magn Reson Med. 2008; 60:822–33. [PubMed: 18816866]
39. Lee L, Sharma S, Morgan B, et al. Biomarkers for assessment of pharmacologic activity for a vascular endothelial growth factor (VEGF) receptor inhibitor, PTK787/ZK 222584 (PTK/ZK): translation of biological activity in a mouse melanoma metastasis model to phase I studies in patients with advanced colorectal cancer with liver metastases. Cancer Chemother Pharmacol. 2006; 57:761–71. [PubMed: 16172907]
40. Morgan B, Thomas AL, Drevs J, et al. Dynamic contrast-enhanced magnetic resonance imaging as a biomarker for the pharmacological response of PTK787/ZK 222584, an inhibitor of the vascular endothelial growth factor receptor tyrosine kinases, in patients with advanced colorectal cancer and liver metastases: results from two phase I studies. J Clin Oncol. 2003; 21:3955–64. [PubMed: 14517187]
41. Liu G, Rugo HS, Wilding G, et al. Dynamic contrast-enhanced magnetic resonance imaging as a pharmacodynamic measure of response after acute dosing of AG-013736, an oral angiogenesis inhibitor, in patients with advanced solid tumors: results from a phase I study. J Clin Oncol. 2005; 23:5464–73. [PubMed: 16027440]
42. Troprès I, Lamalle L, Péoc'h M, et al. In vivo assessment of tumoral angiogenesis. Magn Reson Med. 2004; 51:533–41. [PubMed: 15004795]
43. Zwick S, Strecker R, Kiselev V, et al. Assessment of vascular remodeling under antiangiogenic therapy using DCE-MRI and vessel size imaging. J Magn Reson Imaging. 2009; 29:1125–33. [PubMed: 19388117]
44. Walker-Samuel S, Boult JK, McPhail LD, et al. Non-invasive in vivo imaging of vessel calibre in orthotopic prostate tumour xenografts. Int J Cancer. 2012; 130:1284–93. [PubMed: 21469141]
45. Gilad AA, Israely T, Dafni H, et al. Functional and molecular mapping of uncoupling between vascular permeability and loss of vascular maturation in ovarian carcinoma xenografts: the role of stroma cells in tumor angiogenesis. Int J Cancer. 2005; 117:202–11. [PubMed: 15880497]

Europe PMC Funders Author Manuscripts

46. Gross S, Gilead A, Scherz A, et al. Monitoring photodynamic therapy of solid tumors online by BOLD-contrast MRI. Nat Med. 2003; 9:1327–31. [PubMed: 14502284]
47. Cai K, Shore A, Singh A, et al. Blood oxygen level dependent angiography (BOLDangio) and its potential applications in cancer research. NMR Biomed. 2012; 25:1125–32. [PubMed: 22302557]
48. Kiessling F, Huppert J, Zhang C, et al. RGD-labeled USPIO inhibits adhesion and endocytotic activity of alpha v beta3-integrin-expressing glioma cells and only accumulates in the vascular tumor compartment. Radiology. 2009; 253:462–9. [PubMed: 19789239]
49. Frascione D, Diwoky C, Almer G, et al. Ultrasmall superparamagnetic iron oxide (USPIO)-based liposomes as magnetic resonance imaging probes. Int J Nanomedicine. 2012; 7:2349–59. [PubMed: 22661890]
50. Mulder WJ, Strijkers GJ, van Tilborg GA, et al. Lipid-based nanoparticles for contrast-enhanced MRI and molecular imaging. NMR Biomed. 2006; 19:142–64. [PubMed: 16450332]
51. Mulder WJ, van der Schaft DW, Hautvast PA, et al. Early in vivo assessment of angiostatic therapy efficacy by molecular MRI. FASEB J. 2007; 21:378–83. [PubMed: 17202248]
52. Kiessling F, Morgenstern B, Zhang C. Contrast agents and applications to assess tumor angiogenesis in vivo by magnetic resonance imaging. Curr Med Chem. 2007; 14:77–91. [PubMed: 17266569]
53. Sipkins DA, Cheresh DA, Kazemi MR, et al. Detection of tumor angiogenesis in vivo by alphaVbeta3-targeted magnetic resonance imaging. Nat Med. 1998; 4:623–6. [PubMed: 9585240]
54. Makowski MR, Wiethoff AJ, Blume U, et al. Assessment of atherosclerotic plaque burden with an elastin-specific magnetic resonance contrast agent. Nat Med. 2011; 17:383–8. [PubMed: 21336283]
55. Zhang C, Jugold M, Woenne EC, et al. Specific targeting of tumor angiogenesis by RGD-conjugated ultrasmall superparamagnetic iron oxide particles using a clinical 1.5-T magnetic resonance scanner. Cancer Res. 2007; 67:1555–62. [PubMed: 17308094]
56. Kiessling F, Huppert J, Palmowski M. Functional and molecular ultrasound imaging: concepts and contrast agents. Curr Med Chem. 2009; 16:627–42. [PubMed: 19199927]
57. Iordanescu I, Becker C, Zetter B, et al. Tumor vascularity: evaluation in a murine model with contrast-enhanced color Doppler US effect of angiogenesis inhibitors. Radiology. 2002; 222:460–7. [PubMed: 11818614]
58. Denis F, Bougnoux P, de Poncheville L, et al. In vivo quantitation of tumour vascularisation assessed by Doppler sonography in rat mammary tumours. Ultrasound Med Biol. 2002; 28:431–7. [PubMed: 12049955]
59. Jugold M, Palmowski M, Huppert J, et al. Volumetric high-frequency Doppler ultrasound enables the assessment of early antiangiogenic therapy effects on tumor xenografts in nude mice. Eur Radiol. 2008; 18:753–8. [PubMed: 18084768]
60. Krix M, Kiessling F, Essig M, et al. Low mechanical index contrast-enhanced ultrasound better reflects high arterial perfusion of liver metastases than arterial phase computed tomography. Invest Radiol. 2004; 39:216–22. [PubMed: 15021325]
61. Palmowski M, Lederle W, Gaetjens J, et al. Comparison of conventional time-intensity curves vs. maximum intensity over time for post-processing of dynamic contrast-enhanced ultrasound. Eur J Radiol. 2010; 75:149–53.
62. Rix A, Lederle W, Siepmann M, et al. Evaluation of high frequency ultrasound methods and contrast agents for characterising tumor response to anti-angiogenic treatment. Eur J Radiol. 2012; 81:2710–6. [PubMed: 22093958]
63. Sirsi SR, Flexman ML, Vlachos F, et al. Contrast ultrasound imaging for identification of early responder tumor models to anti-angiogenic therapy. Ultrasound Med Biol. 2012; 38:1019–29. [PubMed: 22425376]
64. Palmowski M, Huppert J, Hauff P, et al. Vessel fractions in tumor xenografts depicted by flow- or contrast-sensitive three-dimensional high-frequency Doppler ultrasound respond differently to antiangiogenic treatment. Cancer Res. 2008; 68:7042–9. [PubMed: 18757418]
65. Krix M, Kiessling F, Vosseler S, et al. Sensitive noninvasive monitoring of tumor perfusion during antiangiogenic therapy by intermittent bolus-contrast power Doppler sonography. Cancer Res. 2003; 63:8264–70. [PubMed: 14678984]

Europe PMC Funders Author Manuscripts

66. Palmowski M, Morgenstern B, Hauff P, et al. Pharmacodynamics of streptavidin-coated cyanoacrylate microbubbles designed for molecular ultrasound imaging. Invest Radiol. 2008; 43:162–9. [PubMed: 18301312]

67. Kiessling F, Fokong S, Koczera P, et al. Ultrasound microbubbles for molecular diagnosis, therapy, and theranostics. J Nucl Med. 2012; 53:345–8. [PubMed: 22393225]

68. Palmowski M, Huppert J, Ladewig G, et al. Molecular profiling of angiogenesis with targeted ultrasound imaging: early assessment of antiangiogenic therapy effects. Mol Cancer Ther. 2008; 7:101–9. [PubMed: 18202013]

69. Palmowski M, Peschke P, Huppert J, et al. Molecular ultrasound imaging of early vascular response in prostate tumors irradiated with carbon ions. Neoplasia. 2009; 11:856–63. [PubMed: 19724679]

70. Pysz MA, Foygel K, Rosenberg J, et al. Antiangiogenic cancer therapy: monitoring with molecular US and a clinically translatable contrast agent (BR55). Radiology. 2010; 256:519–27. [PubMed: 20515975]

71. Bzyl J, Palmowski M, Rix A, et al. The high angiogenic activity in very early breast cancer enables reliable imaging with VEGFR2-targeted microbubbles (BR55). Eur Radiol. 2012 (in press).

72. Eisenblätter M, Höltke C, Persigehl T, et al. Optical techniques for the molecular imaging of angiogenesis. Eur J Nucl Med Mol Imaging. 2010; 37(Suppl 1):127–37.

73. Ale A, Ermolayev V, Herzog E, et al. FMT-XCT: in vivo animal studies with hybrid fluorescence molecular tomography-X-ray computed tomography. Nat Methods. 2012; 9:615–20. [PubMed: 22561987]

74. Kunjachan S, Gremse F, Theek B, et al. Non-invasive optical imaging of nanomedicine biodistribution. ACS Nano. 2012 (in press).

75. Zhang Q, Bindokas V, Shen J, et al. Time-course imaging of therapeutic functional tumor vascular normalization by antiangiogenic agents. Mol Cancer Ther. 2011; 10:1173–84. [PubMed: 21586628]

76. Lederle W, Arns S, Rix A, et al. Failure of annexin-based apoptosis imaging in the assessment of antiangiogenic therapy effects. EJNMMI Res. 2011; 1:26. [PubMed: 22214377]

77. Chang SK, Rizvi I, Solban N, et al. In vivo optical molecular imaging of vascular endothelial growth factor for monitoring cancer treatment. Clin Cancer Res. 2008; 14:4146–53. [PubMed: 18593993]

78. Wang H, Chen K, Niu G, et al. Site-specifically biotinylated VEGF(121) for near-infrared fluorescence imaging of tumor angiogenesis. Mol Pharm. 2009; 6:285–94. [PubMed: 19099493]

79. Terwisscha van Scheltinga AG, van Dam GM, Nagengast WB, et al. Intraoperative near-infrared fluorescence tumor imaging with vascular endothelial growth factor and human epidermal growth factor receptor 2 targeting antibodies. J Nucl Med. 2011; 52:1778–85. [PubMed: 21990576]

80. Snoeks T, Löwik C, Kaijzel E. In vivo optical approaches to angiogenesis imaging. Angiogenesis. 2010; 13:135–47. [PubMed: 20449766]

81. Zhang N, Fang Z, Contag PR, et al. Tracking angiogenesis induced by skin wounding and contact hypersensitivity using a Vegfr2-luciferase transgenic mouse. Blood. 2004; 103:617–26. [PubMed: 14512298]

82. Kishimoto J, Ehama R, Ge Y, et al. In vivo detection of human vascular endothelial growth factor promoter activity in transgenic mouse skin. Am J Pathol. 2000; 157:103–10. [PubMed: 10880381]

83. Wang Y, Iyer M, Annala A, et al. Noninvasive indirect imaging of vascular endothelial growth factor gene expression using bioluminescence imaging in living transgenic mice. Physiol Genomics. 2006; 24:173–80. [PubMed: 16410544]

84. Wang LV, Hu S. Photoacoustic tomography: in vivo imaging from organelles to organs. Science. 2012; 335:1458–62. [PubMed: 22442475]

85. Laufer J, Zhang E, Raivich G, et al. Three-dimensional noninvasive imaging of the vasculature in the mouse brain using a high resolution photoacoustic scanner. Appl Opt. 2009; 48:D299–306. [PubMed: 19340121]

86. De la Zerda A, Zavaleta C, Keren S, et al. Carbon nanotubes as photoacoustic molecular imaging agents in living mice. Nat Nanotechnol. 2008; 3:557–62. [PubMed: 18772918]

Europe PMC Funders Author Manuscripts

87. Cai X, Li L, Krumholz A, et al. Multi-scale molecular photoacoustic tomography of gene expression. PLoS One. 2012; 7:e43999. [PubMed: 22952846]

88. Cai W, Chen X. Multimodality molecular imaging of tumor angiogenesis. J Nucl Med. 2008; 49(Suppl 2):113S–28S. [PubMed: 18523069]

89. Cai W, Chen K, Mohamedali KA, et al. PET of vascular endothelial growth factor receptor expression. J Nucl Med. 2006; 47:2048–56. [PubMed: 17138749]

90. Cao F, Li Z, Lee A, et al. Noninvasive de novo imaging of human embryonic stem cell-derived teratoma formation. Cancer Res. 2009; 69:2709–13. [PubMed: 19318556]

91. Liu Z, Jia B, Zhao H, et al. Specific targeting of human integrin (v) (3) with (111)In-labeled Abegrin™ in nude mouse models. Mol Imaging Biol. 2011; 13:112–20. [PubMed: 20383594]

92. Jia B, Shi J, Yang Z, et al. 99mTc-labeled cyclic RGDfK dimer: initial evaluation for SPECT imaging of glioma integrin alphavbeta3 expression. Bioconjug Chem. 2006; 17:1069–76. [PubMed: 16848417]

93. Yang M, Gao H, Yan Y, et al. PET imaging of early response to the tyrosine kinase inhibitor ZD4190. Eur J Nucl Med Mol Imaging. 2011; 38:1237–47. [PubMed: 21360246]

94. Jin ZH, Furukawa T, Claron M, et al. Positron emission tomography imaging of tumor angiogenesis and monitoring of antiangiogenic efficacy using the novel tetrameric peptide probe (64)Cu-cyclam-RAFT-c(-RGDfK-) (4). Angiogenesis. 2012; 15:569–80. [PubMed: 22644563]

95. Jati A, Tatlı S, Morgan JA, et al. Imaging features of bone metastases in patients with gastrointestinal stromal tumors. Diagn Interv Radiol. 2012; 18:391–6. [PubMed: 22407696]

96. Schwarzenberg J, Czernin J, Cloughesy TF, et al. 3 deoxy-3 18F-fluorothymidine PET and MRI for early survival predictions in patients with recurrent malignant glioma treated with bevacizumab. J Nucl Med. 2012; 53:29–36. [PubMed: 22159180]

97. Metz S, Ganter C, Lorenzen S, et al. Phenotyping of tumor biology in patients by multimodality multiparametric imaging: relationship of microcirculation, alphavbeta3 expression, and glucose metabolism. J Nucl Med. 2010; 51:1691–8. [PubMed: 20956471]

98. Bach-Gansmo T, Danielsson R, Saracco A, et al. Integrin receptor imaging of breast cancer: a proof-of-concept study to evaluate 99mTc-NC100692. J Nucl Med. 2006; 47:1434–9. [PubMed: 16954550]

99. Van der Veldt AA, Lubberink M, Bahce I, et al. Rapid decrease in delivery of chemotherapy to tumors after anti-VEGF therapy: implications for scheduling of anti-angiogenic drugs. Cancer Cell. 2012; 21:82–91. [PubMed: 22264790]

100. Fokong S, Theek B, Wu Z, et al. Image-guided, targeted and triggered drug delivery to tumors using polymer-based microbubbles. J Control Release. 2012; 163:75–81. [PubMed: 22580225]

Europe PMC Funders Author Manuscripts

Europe PMC Funders Author Manuscripts

Europe PMC Funders Author Manuscripts

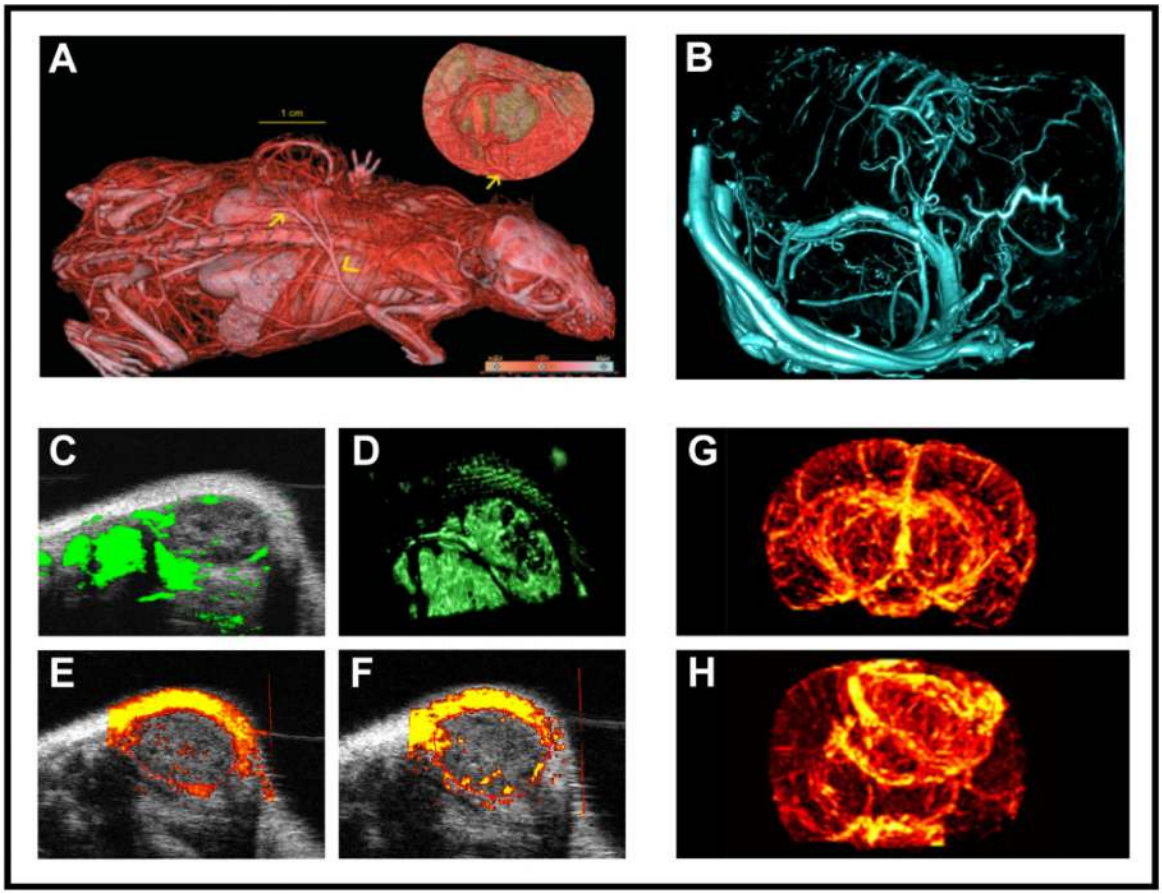

Figure 1. Micro-morphological imaging of tumor angiogenesis

A: *In vivo* visualization of tumor blood vessels in a subcutaneously implanted HaCaTras-A-5RT3 squamous cell carcinoma xenograft using contrast-enhanced μCT in combination with an iodine-based contrast agent [19]. **B:** For a highly resolved 3D visualization of the micromorphology of tumor blood vessels, tumor-bearing mice can be perfused with Microfil®, a lead-containing CT contrast agent which polymerizes intravascularly. After perfusion, excised tumors are scanned using an ultra-high resolution μCT scanner resulting in a resolution of less than 10 μm voxel side length. **C-F:** For rapid morphological imaging of blood microvessels in subcutaneous tumors, 3D contrast-enhanced US before (**C**) and after volume rendering (**D**), Power Doppler US (**E**) and contrast-enhanced Power Doppler US (**F**) can be used. **G-H:** Finally, MR angiography techniques using Blood Oxygen Level Dependent (BOLD) imaging enable the visualization of the 3D vascular network of tumors. After inducing hypoxia via the inhalation of 8% oxygen, BOLD contrast generates high-resolution maps of normal brain (**G**) and tumor brain vasculature (**H**) using a 9.4 Tesla scanner. For investigating micro-morphological aspects, maximum intensity projection (MIP) images can be obtained, which clearly show differences in symmetry and density of blood vessels in brain tumors vs. healthy brain tissue (reproduced with permission from [47]).

Europe PMC Funders Author Manuscripts

Europe PMC Funders Author Manuscripts

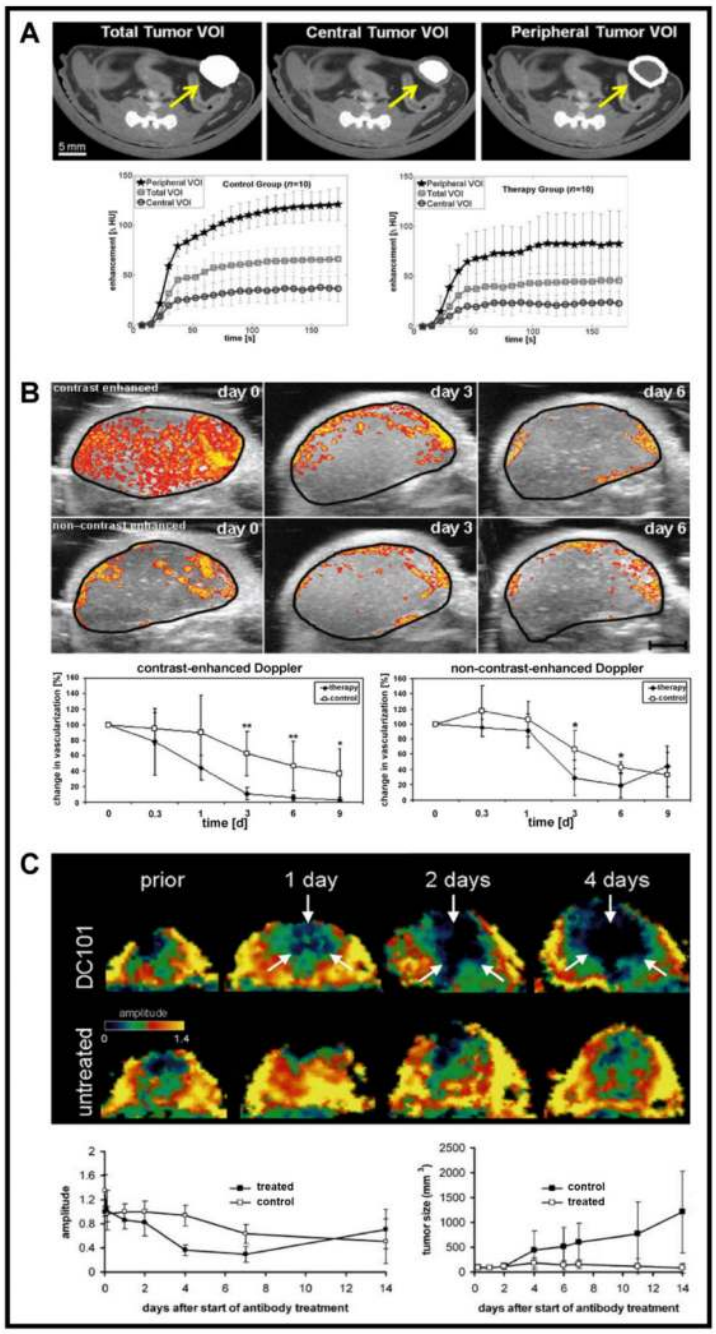

Figure 2. Functional imaging of tumor angiogenesis

A: Dynamic CT imaging is highly suitable for assessing anti-angiogenic therapy effects. During the CT scan, a blood pool contrast agent is injected intravenously. After tumor segmentation and determination of different volumes of interest (VOI) within the tumor (e.g. total tumor volume vs. tumor center vs. tumor periphery), dynamic contrast-enhanced CT imaging can be employed to longitudinally quantify differences between treated and non-treated animals (reproduced from [20] with kind permission from Springer Science + Business Media). **B**: Another method for non-invasively assessing anti-angiogenic therapy effects, especially those depending on the maturity of tumor blood vessels, relies on the combination of contrast-enhanced and non-contrast-enhanced high-frequency volumetric

Europe PMC Funders Author Manuscripts

Europe PMC Funders Author Manuscripts

Power Doppler US. Because contrast-sensitive US is more sensitive for small immature vessels (primarily in the tumor center in this particular example), whereas flow-sensitive non-contrast-enhanced US mostly captures large and mature vessels (primarily in the tumor periphery), the combination of both methods can provide non-invasive feedback on blood vessel maturation in tumors during anti-angiogenic treatment. As early as 3 days after the beginning of anti-angiogenic treatment with sunitinib in mice with subcutaneously inoculated A431 tumors, a regression of immature vessels in the tumor center can be observed, while large and mature vessels at the tumor periphery are only partially affected (data from [64]). **C**: A third modality which is highly suitable for visualizing and quantifying anti-angiogenic therapy effects is DCE-MRI. Upon treating mice bearing subcutaneous squamous cell carcinoma xenografts, anti-angiogenic therapy with the VEGFR-2-blocking antibody DC 101, representative parameter maps of the amplitude A were acquired over a 4 day period. Changes in the amplitude, assessed using the Brix model, are shown in the lower left panel, and were compared with changes in tumor volume (lower right panel). This comparison clearly shows that therapy effects can be observed much earlier when monitoring changes in the amplitude. At later time points, when treated tumors had decreased in volume while non-treated tumors had increased, amplitude levels re-increased in treated tumors, and were even higher than in non-treated tumors. This can be explained by the fact that resorption of central tumor parts had occurred upon anti-angiogenic therapy, and that large and mature vessels from the tumor periphery had drawn closer together (reproduced from [36], with permission from Neoplasia).

Europe PMC Funders Author Manuscripts

Europe PMC Funders Author Manuscripts

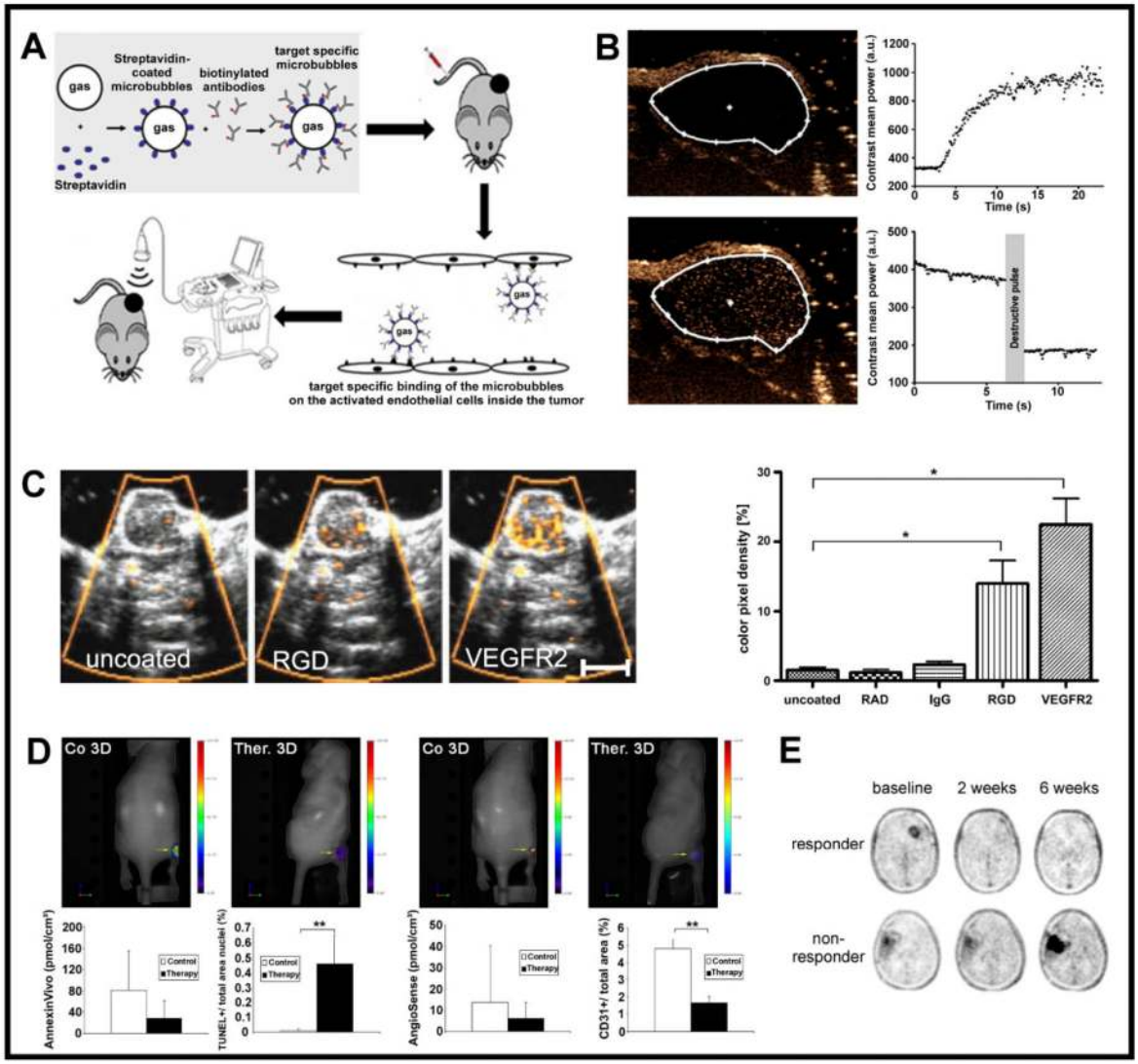

Figure 3. Molecular imaging of tumor angiogenesis

A: Schematic setup of molecular US imaging in subcutaneous mouse tumors using antibody-functionalized microbubbles (MB), which specifically bind to angiogenesis-associated markers, such as VEGFR-2 or $\alpha_v\beta_3$ integrins. **B**: Example for the *in vivo* quantification of VEGFR-2-targeted MB binding to angiogenic blood vessels in subcutaneous CT26 tumors. Before MB injection, hardly any signal is detected in tumors (upper left panel). Contrast agent injection leads to an increase of signal intensity due to inflowing MB, confirming efficient tumor perfusion (upper right panel). After waiting for seven minutes, a significant amount of VEGFR2-targeted MB can be observed within the tumor (lower left panel). Upon reaching a plateau phase (of 400 a.u. in this example), a high-mechanical index destructive US pulse is applied, which destroys all MB (lower right panel). The difference in signal intensity before and after application of this destructive US pulse correlates with the amount of bound MB, and therefore with the expression levels of VEGFR-2 (A and B reprinted from [100] with permission from Elsevier). **C**: Using SPAQ technique, the expression levels of VEGFR-2 or $\alpha_v\beta_3$ were assessed in squamous cell carcinoma xenografts (HaCaT-ras-A-5RT3) in mice. Hardly any accumulation of uncoated,

RAD- and IgG-targeted control MB was observed using Power Doppler US; RGD- or VEGFR-2-targeted MB, on the other hand, showed prominent binding to tumor blood vessels (data from [68]). **D**: Fluorescense-based molecular imaging of apoptosis and angiogenesis using FMT. In sunitinib-treated vs. non-treated A431 tumor-bearing mice, apoptosis was non-invasively investigated using *Annexin Vivo 750*, a near-infrared fluorescence probe that selectively binds to cell membranes during the early stages of apoptosis. Tumor vascularization was investigated using *AngioSense 680*, a blood pool marker. While vascularization significantly decreased in treated tumors, no enhanced annexin accumulation was observed although the gold standard TUNEL staining indicated an increased apoptosis rate (data form [76]). **E**: Representative examples of longitudinal malignant glioma monitoring using ^{18}F-FLT PET in patients treated with bevacizumab. The FLT-uptake at baseline was determined before treatment. At later time points, ^{18}F-FLT PET imaging can be used to discriminate responders from non-responders and ^{18}F-FLT tumor uptake changes at 2 and 6 weeks were significant predictors of progression-free survival by Kaplan-Meier analysis ($P < 0.001$) (reprinted by permission of the Society of Nuclear Medicine from [96], figure 1).

Europe PMC Funders Author Manuscripts

Europe PMC Funders Author Manuscripts

Europe PMC Funders Author Manuscripts

Europe PMC Funders Author Manuscripts

Table 1

In vivo imaging modalities and their suitability for morphological, functional and molecular vascular imaging

Modality	Morphological Imaging	Functional Imaging	Molecular Imaging
CT	+ +	+	–
US	+	++	++
MRI	+	++	+/–
OI (FMT)	–	+	++
PET	–	+	++
SPECT	–	+	++

Europe PMC Funders Author Manuscripts

Europe PMC Funders Author Manuscripts

Table 2

Overview of imaging modalities and their characteristics

Modality	Advantages	Disadvantages	Contrast Agents
CT	• High resolution (~ 20 - 200 μm) • Unlimited penetration depth • Rapidly operable • User independent • Low cost	• Insufficient soft tissue contrast without contrast agent application • Radiation effects • Low sensitivity to contrast agents	• Iodine-based clinical contrast agents (e.g. Imeron, Omnipaque, Ultravist) • Polyiodinated triglyceride emulsions • Barium-based nanoparticles • Gold-based nanoparticles
US	• High temporal and spatial resolution (~ 50 - 100 μm) • Rapidly operable, real time imaging • Low cost	• User dependent • Not suitable for whole body imaging	• Unspecific or target-specific Gas-filled microbubbles
MRI	• Excellent soft tissue contrast • High spatial resolution (~ 10 - 500 μm) • Unlimited penetration depth • Multiple methods to characterize vessels • Reporter gene imaging possible	• Non-rapidly operable • Relatively low sensitivity for contrast agents • High costs	• Gadolinium-containing chelate complexes • Paramagnetic liposomes and polymers • USPIO • Carbogen/oxygen • Fluorinated probes
OI (ORI, FMT)	• High sensitivity for contrast agents • Wide range of probes • Activatable probes • Reporter gene imaging • Low costs	ORI: • Surface-weighted, low penetration depth (< 10 cm) • High background signal FMT: • Sensitive to artifacts • Not as quantitative as PET and SPECT yet	• Near-infrared fluorochromelabeled biomolecules • Quenched activatable probes • Quantum dots • Fluorescent proteins • Luciferin/luciferase
PAI	• High sensitivity • Quantitative • Real time imaging possible • Low costs	• Lack of optimal contrast agents • Limited penetration depth	• Dyes • Nanoparticles (e.g. gold-NPs, gold nanorods, carbonanotubes) • Fluorescent proteins
PET	• Unlimited penetration depth • Very high sensitivity • Quantitative	• Low spatial resolution (1-2mm) • No morphological information • Radiation exposure • Very high costs	• Molecules labeled with beta plus emitting radioisotopes

Modality	Advantages	Disadvantages	Contrast Agents
SPECT	• Unlimited penetration depth • Very high sensitivity • Long-living radionucleotides	• Low spatial resolution (1-2mm) • No morphological information • Radioactivity of the probes • High costs	• Molecules labeled with gamma-emitting radionucleotides

Europe PMC Funders Author Manuscripts

Europe PMC Funders Author Manuscripts

Europe PMC Funders Author Manuscripts

Europe PMC Funders Author Manuscripts

Table 3

Overview of vascular parameters that are often assessed using dynamic contrast-enhanced ( )CT and MRI and their biological relevance

Parameter	Biological Relevance
amplitude *A* [a.u.]	• Two Compartment Model (Brix) • Maximal signal intensity • Strong dependency on perfusion and rBV • Rapidly decreasing during initial phase of anti-angiogenic therapy due to tumor blood vessel regression
area under curve (AUC) [a.u.]	• Is the integral of a curve resulting from the signal intensity as a function of time • Is a mixed parameter of perfusion and rBV • Is initially increased in tumors due to a high MVD • Is decreased under anti-angiogenic therapy because of regression of tumor blood vessels
BF [ml min^{-1}]	• Indicates how much blood (ml) flows per tissue mass (g) per time (min) • Is decreased under anti-angiogenic therapy because of tumor blood vessel regression
K_{ep} [min^{-1}]	• Two Compartment Model (Brix) • Efflux volume transfer constant of a contrast agent from the interstitial compartment to the vascular compartment in a pharmacokinetic two-compartment model • Major dependency on vessel permeability and perfusion • Variable change under anti-angiogenic therapy
K_{trans} [min^{-1}]	• Two Compartment Model (Tofts) • Influx volume transfer constant of a contrast agent from the vascular compartment to the interstitial compartment • Major dependency on perfusion, minor dependency on permeability • Is decreased under anti-angiogenic therapy because of tumor blood vessel regression
mean transit time (MTT) [s]	• Indicates how long a contrast agent bolus needs to pass from a feeding artery through the tissue of interest (e.g. tumor) in a venous/draining vessel • Correlates with tissue perfusion • Is decreased under anti-angiogenic therapy because of tumor blood vessel regression
perfusion [ml^{-1} min^{-1} (100 g)$^{-1}$]	• Is characterized as the blood supply of various tissues including organs or tumors • Is increased in tumors due to a high arterial feeding, high vessel density and high vessel permeability • Is decreased under anti-angiogenic therapy because of tumor blood vessel regression
rBV [%]	• Percentage of the blood volume to the total tumor volume • Correlates with the amount of functional blood vessels within a tumor • Is decreased under anti-angiogenic therapy because of tumor blood vessel regression
vascular permeability [min^{-1} ml^{-1}]	• Depends on the contrast agent/ molecule properties, vessel surface area, vessel leakiness and the size of the interstitial distribution space • Is also used synonymously as capillary permeability • Vascular permeability is high in tumors with mainly immature, leaky blood vessels

Parameter	Biological Relevance
	• Decreases in tumors with mainly immature, leaky vessels under anti-angiogenic therapy because of vessel regression/increasing vessel maturity
V_e [%]	• Two Compartment Model (Tofts) • Is the extravascular, extracellular leakage space volume as a fraction of the whole tumor volume • Strong dependency on both interstitial and plasma volume

Europe PMC Funders Author Manuscripts

Europe PMC Funders Author Manuscripts

Europe PMC Funders Author Manuscripts
Europe PMC Funders Author Manuscripts

Table 4

Examples of non-invasive imaging studies assessing anti-angiogenic therapy effects

Imaging Modality	Contrast Agent	Determined Parameter	Antiangiogenic Agent	Mechanism of Action	Setting	Assessed Effects in the Therapy vs. Control Group	Ref.
DCE- CT	• Ultravist 300 (500 mg iodine/kg bolus in 2 s)	• total tumor volume [cm^3] • rBV [%] • vascular permeability K [min^{-1} ml^{-1}] • AUC [HU]	• everolimus (10 mg, thrice per week)	mTOR inhibitor	• MCF7 mammary cancer xenografts	• total tumor volume P = 0.001 • rBV P = 0.029 - 0.136 * • K P = 0.032 - 0.243 * • AUC P = 0.007 - 0.023 * * Depending on the segmented region of the tumor (total vs. peripheral vs. central). Most significant differences were observed in the tumor periphery.	[20]
DCE- CT	• Omnipaque 300 (2.2 /g)	• total tumor volume [cm^3] • BF [ml/min per 100 g] • BV [ml/100 g] • MTT [s] • PS (permeability surface area product) [ml/min per 100 g]	• vanetinib (50 mg/kg, 2 applications in 24 hours)	multi-targeted receptor tyrosine kinase inhibitor	• LoVo colon adenocarcinoma xenografts	Nonhypovascular tumors: • total tumor volume P > 0.05 • BF P < 0.05 • BV P < 0.05 • MTT P > 0.05 • PS P > 0.05 Hypovascular tumors showed no significant differences	[21]
Ex vivo high-resolution CT	• Microfil	• MVD [%] • relative vessel volume • vascular branching by tree analysis	• bevacizumab (5 mg/ 200 over 24 h continuously per pump for 14 d)	humanized monoclonal anti-VEGF-A antibody	• A549 orthotopic lung adenocarcinomic xenografts	• MVD P < 0.0001 • relative vessel volume P <0.05 • substantially less branching points at smaller vessel diameters (<25 mm^2)	[25]

Europe PMC Funders Author Manuscripts
Europe PMC Funders Author Manuscripts

Imaging Modality	Contrast Agent	Determined Parameter	Antiangiogenic Agent	Mechanism of Action	Setting	Assessed Effects in the Therapy vs. Control Group	Ref.
DCE-MRI	• **Magnevist** (0.4 mmol/kg Gd-DTPA bolus in 5s)	• ***K_{ep}*** **(exchange rate constant)** based on the pharmacokinetic two-compartment model of Brix • ***amplitude A*** (increase of signal intensity relative to precontrast value	• **DC101** (800 μg i.p. thrice a week)	**VEGFR-2 antibody**	• **HaCaT-ras-A-5RT3 skin squamous cell carcinoma xenografts**	• ***A*** **rapidly during initial phase of anti-angiogenic therapy (4 days)** • **differences in tumor volumes were not significant during the initial phase** • **later, when treated tumors had decreased in volume while non-treated tumors had continuously increased their volumes, *A* re-increased in treated tumors** • **no significant differences for K_{ep} for the whole examination period**	[36]
VSI MRI	• **very small superparamagnetic iron oxid nanoparticles** (200 μmol Fe/kg)	• **vessel size index (VSI)**	• **sunitinib for A431** (60mg/kg i.p.) • **bevacizumab for HaCaT-ras- A-5RT3** (1mg i.p. twice a week)	**multi-targeted receptor tyrosine kinase inhibitor & humanized monoclonal anti-VEGF-A antibody**	• **A431 epidermoid carcinoma xenografts** • **HaCaT-ras-A-5RT3 skin squamous cell carcinoma xenografts**	• **VSI ↓ in sunitinib treated A431 tumors ($P < 0.05$)** • **no significant changes in VSI in bevacizumab treated HaCaT-ras-A-5RT3 tumors**	[43]
Bold MRI	generated contrast by photo-consumption of oxygen and hemodynamic effects resulting from PDT application	• **T_2-weighted MRSI (magnetic resonance signal intensity) [% of baseline at t_0]** • **ΔR_2^* (defined as R_2^* illumination**	• **simultaneous TOOKAD** (5 mg/kg) **and transcutaneous PDT**	**TOOKAD: photo-sensitizing, vascular disrupting agent**	• **M2R melanoma xenografts**	• **MRSI ↓** • **rapid increase of ΔR_2^* in treated tumors** • **rapid decrease of**	[46]

Europe PMC Funders Author Manuscripts
Europe PMC Funders Author Manuscripts

Imaging Modality	Contrast Agent	Determined Parameter	Antiangiogenic Agent	Mechanism of Action	Setting	Assessed Effects in the Therapy vs. Control Group	Ref.
		minus R_2* pre illumination) [1/s]				R_2* in untreated tumors	
Volumetric Power Doppler Ultrasound	• bolus injection of 100 of MB	• tumor volume • color pixel density	• sunitinib (80 mg/kg daily i.p.)	multi-targeted receptor tyrosine kinase inhibitor	• A431 epidermoid carcinoma xenografts	• tumor volume over time ($P < 0.05$ at day 3 and $P < 0.01$ at day 6) • in contrast-enhanced scans color pixel density rapidly ($P < 0.01$ at day 3) • in non-contrast-enhanced scans color pixel density slowly but then reincreases indicating that different vessel fractions were captured with each of this methods (see figure 2B)	[64]
Power Doppler Ultrasound	• bolus injection of 100 of galactose-based US contrast agent (300 mg/ml Levovist)	• blood volume • blood flow • perfusion (i.e. blood flow normalized to tissue volume) • mean blood velocity	• DC101 (800 g i.p. thrice a week)	VEGFR-2 antibody	• HaCaT-ras-A-5RT3 skin squamous cell carcinoma xenografts	• reduction in tumor vasculature was assessable before a reduction in tumor size became visible • blood volume in treated and in untreated animals • blood flow $P < 0.05$ • mean blood velocity but no significance • central tumor perfusion in treated and	[65]

Europe PMC Funders Author Manuscripts
Europe PMC Funders Author Manuscripts

Imaging Modality	Contrast Agent	Determined Parameter	Antiangiogenic Agent	Mechanism of Action	Setting	Assessed Effects in the Therapy vs. Control Group	Ref.
						in untreated animals	
Power Doppler Ultrasound	• **□v□3-specific MB** • **ICAM-1-specific MB** (injection of 300 □ of a 10^8 MB/ml suspension)	• **color pixel density**	• **16-Gy single dose of ^{12}C**	**DNA damage**	• **AT-1 prostate cancer xenografts**	• **color pixel density □by using □v□3-specific MB in irradiated tumors after 3 days (*P* < 0.05)** • **color pixel density for ICAM-1-specific MB showed no significant changes**	[69]
OI - FMT	• **Annexin Vivo 750** (2 nmol 2 h prior imaging) • **AngioSense 680** (2 nmol 2 h immediately before imaging)	• **Annexin Vivo accumulation (specific for apoptotic cells)** • **AngioSense accumulation (blood pool marker)**	• **sunitinib** (50 mg/kg daily i.p.)	**multi-targeted receptor tyrosine kinase inhibitor**	• **A431 epidermoid carcinoma xenografts**	• **Annexin Vivo accumulation □*P* = 0.13 (contradictory to high apoptotic rates proven by TUNEL staining)** • **AngioSense accumulation □*P* = 0.51 (in tendency in line with CD31 area fraction, *P* < 0.001)**	[76]
PET	• **^{18}F-FDG** • **^{18}F-FLT** • **^{18}F-FPPRGD2** (1.85 MBq per mouse)	• **glucose metabolism specific 18F-FDG uptake** • **proliferation specific ^{18}F-FLT uptake** • **□v□3 integrin-specific ^{18}F-FPPRGD2 Uptake**	• **ZD4190** (100 mg/kg orally per day for three days)	**VEGFR-2 tyrosine kinase inhibitor**	• **MDA-MB-435 orthotopic breast carcinoma xenografts**	• **no significant changes in ^{18}F-FDG uptake** • **^{18}F-FLT uptake □ during initial phase of anti-angiogenic therapy (at day 3, *P* < 0.001)** • **^{18}F-FPPRGD2 uptake □ during initial phase of anti-angiogenic**	[93]

Europe PMC Funders Author Manuscripts
Europe PMC Funders Author Manuscripts

Imaging Modality	Contrast Agent	Determined Parameter	Antiangiogenic Agent	Mechanism of Action	Setting	Assessed Effects in the Therapy vs. Control Group	Ref.
						therapy (at day 3, $P < 0.001$), then re-increase back to baseline	
PET	• ^{18}F-FLT (2.0 MBq/kg)	• proliferation specific ^{18}F-FLT SUV (standardized uptake value)	• bevacizumab & irinotecan	humanized monoclonal anti-VEGF-A antibody & topoisomerase I inhibitor	• 30 Glioma patients	• ^{18}F-FLT tumor uptake ↓in responder (46±14 %) vs. ^{18}F-FLT uptake ↓in non-responder (20±52 %); $P = 0.001$ • ^{18}F-FLT tumor uptake changes at 2 and 6 weeks were significant predictors of progression-free and overall survival by Kaplan-Meier analysis ($P < 0.001$); sensitivity: 82%; specificity: 80%	[96]